Magnetic neutron scattering measurements on a single crystal of frustrated $ZnFe_2O_4$

K. Kamazawa and Y. Tsunoda
Department of Applied Physics, School of Science and Engineering, Waseda University, 3-4-1 Ohkubo, Shinjuku, Tokyo 169-8555, Japan

H. Kadowaki
Department of Physics, Tokyo Metropolitan University, Hachioji-shi, Tokyo 192-0397, Japan

K. Kohn
Department of Physics, School of Science and Engineering, Waseda University, 3-4-1 Ohkubo, Shinjuku, Tokyo 169-8555, Japan
(Received 19 June 2002; revised manuscript received 15 January 2003; published 22 July 2003)

Single crystals of $ZnFe_2O_4$ are investigated with neutron scattering measurements from the viewpoint of geometrical frustration. Magnetic diffuse scattering was distributed along the first Brillouin zone boundary of the fcc structure. The results show that the frustration occurs between the antiferromagnetically coupled third-neighbor spins, rather than between the similarly coupled first-neighbor spins. In addition, another type of diffuse scattering was found around some nuclear Bragg peak positions. This indicates that the first-neighbor exchange interaction in the 90° configuration is ferromagnetic rather than antiferromagnetic. Energy spectra were investigated at several points. The unusual magnetic behavior originates from the geometrical frustration and a unique property of the first-neighbor interaction.

DOI: 10.1103/PhysRevB.68.024412 PACS number(s): 75.50.Ee, 75.40.Gb, 75.50.Lk, 61.12.Ld

I. INTRODUCTION

$ZnFe_2O_4$ has a normal spinel structure composed of 8 tetrahedral *A* sites and 16 octahedral *B* sites. The *A* and *B* sites are occupied by Zn^{2+} and Fe^{3+} ions, respectively. The *B* sites of this structure have a special atomic arrangement, whereby the corresponding *B* cations are located at the corners of the tetrahedron, while each corner is shared by two tetrahedra. If the tetrahedron is regarded as a single molecule, then the *B* sites of the spinel structure can be described as an fcc configuration of molecules (see Fig. 1). (The third-neighbor Fe^{3+} ions can also be regarded as an fcc configuration.) The tetrahedral network has the same atomic configuration as that of various pyrochlores and $C15$ intermetallic Laves phase compounds, such as $Y(Sc)Mn_2$, systems which are well known in terms of three-dimensional geometrical frustration, and their unusual ground states, e.g., spin glass,[1–3] spin ice,[4–6] spin liquid, and others.[7–11]

It is thought that $ZnFe_2O_4$ is antiferromagnetic, with a Néel temperature of about 10 K.[12–17] However, estimates based on magnetic susceptibility give a Curie-Weiss temperature of about +100 K. Therefore, strong spin frustration is also expected in $ZnFe_2O_4$.[18,19] Several authors[13–17] have performed powder neutron diffraction measurements. Nevertheless, details are still unclear, because data obtained from powder samples provide inadequate information concerning the exact location of diffuse scattering. Our success in growing single crystals, of sufficient size for neutron scattering measurements, enabled us to clarify the unusual magnetic behavior of $ZnFe_2O_4$ from the viewpoint of geometrical frustration. It also made possible the determination of the exact location of diffuse scattering in reciprocal space. In addition, energy spectra were investigated at several points.

Before discussing the main topic of this paper, we emphasize that the present experiments were performed on a high-quality sample of $ZnFe_2O_4$, in such a way that its unusual magnetic behavior was treated as an intrinsic property. This is noted here because previous reports[20–23] have argued that sample imperfections are the cause of this unusual magnetic behavior. In these cases, the specimens seemed to be in a metastable state, since the coexistence of short-range order, as well as long-range order, probably due to sample heterogeneity, was observed. It is our experience, that when the specimens are carefully purified during preparation, they do not show any well-defined Bragg peaks corresponding to the formation of long-range order. In our view, this material remains intrinsically disordered even at the lowest observable temperature (1.5 K). This point has already been clarified and reported in Ref. 24.

II. SAMPLE PREPARATION AND EXPERIMENTAL METHOD

Single crystals of $ZnFe_2O_4$ were grown by the flux method, and the maximum temperature during the process was 1250 °C. Initially, the $ZnFe_2O_4$ compound was synthesized by the usual solid solution, which was then used to grow the single crystals. The lattice parameter $a=8.52$ Å at ambient temperature, was determined by x-ray powder diffraction. Various values of this parameter have been reported (e.g., $a=8.439$ Å,[15] $a=8.4599$ Å,[16] and $a=8.43$ Å,[21] etc.) However, its present value is more accurate, since it is obtained from a high-quality sample (see Ref. 24). A batch of single crystals was found at the bottom of the platinum crucible. Several of the octahedral crystals had edges of length 5–7 mm, and a few had lengths as large as 10–15 mm.

Two spectrometers were used in the present neutron scattering measurements. Magnetic diffuse scattering was detected with the high-*Q*-resolution (HQR) triple-axis spectrometer installed at the T1 thermal guide of JEARI. The wave vector k_i of the incident neutrons was 2.5579 $Å^{-1}$. A pyrolitic graphite (PG) analyzer and a thick PG filter were

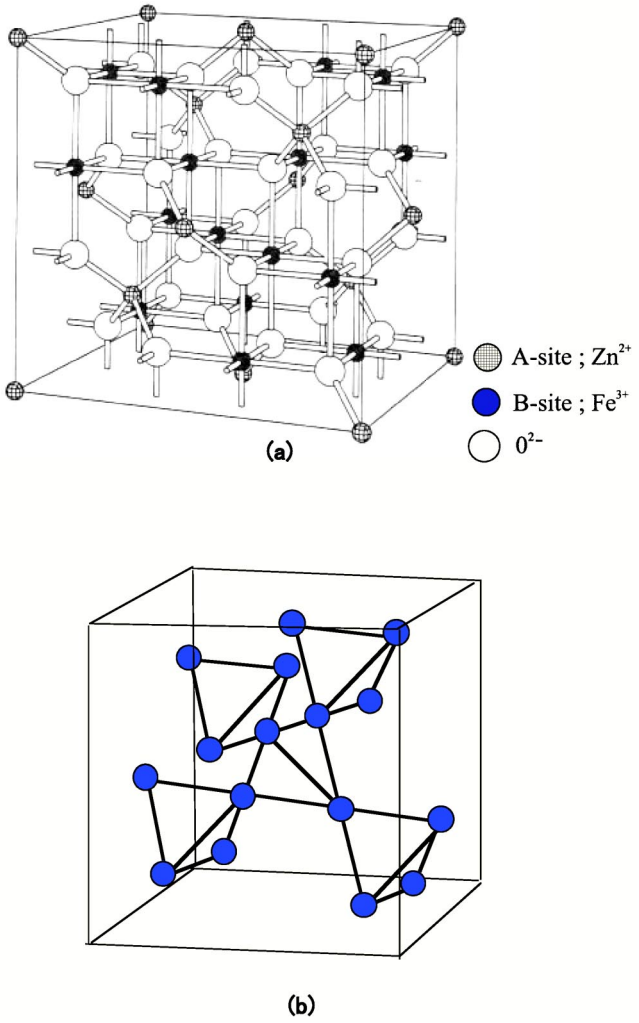

FIG. 1. (a) Normal spinel structure of $ZnFe_2O_4$. (b) Fe^{3+} arrangement on *B* sites, showing corner-sharing tetrahedra. The tetrahedra form the fcc structure.

used to obtain a full-width at half maximum (FWHM) of energy resolution equal to 0.66 meV. Since the diffuse scattering data were taken with the analyzer, the spin motion, with characteristic time shorter than 10^{-11} sec, was discarded as an inelastic scattering process. On the other hand, energy spectra were obtained with the high-energy-resolution (HER) triple-axis spectrometer installed at the C1 cold guide of JEARI. Two scattered neutron wave vectors k_f, namely, 1.4725 and 1.0815 $Å^{-1}$, were used here. The FWHM for each of these was estimated to be 0.166 and 0.0498 meV, respectively. The data were taken in the constant-k_f mode of operation with a horizontally focusing analyzer for enhancement of the data collection rate. The spin motion, with characteristic time shorter than 10^{-10} sec, was again discarded as an inelastic scattering process.

Magnetic susceptibility measurements were performed with a SQUID system at the Materials Characterization Central Laboratory in Waseda University. For this purpose, the sample consisted of the crystals grown in the same crucible as that used for neutron scattering. The magnetic field was applied along the ⟨001⟩ axis. Field-cooled (FC) and zero-field-cooled (ZFC) processes were studied with magnetic fields of 200 and 500 Oe in the temperature range between 5 and 700 K.

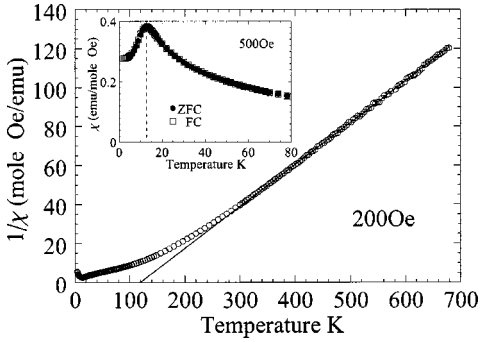

FIG. 2. The temperature dependence of the inverse magnetic susceptibility $1/\chi$ in a magnetic field ($H=200$ Oe). The inset shows the zero-field-cool (ZFC) and field-cool (FC) magnetic susceptibility χ in a magnetic field ($H=500$ Oe).

III. EXPERIMENTAL RESULTS

A. Magnetic susceptibility

The temperature dependence of the magnetic susceptibility (inset) and its inverse susceptibility are shown in Fig. 2. At first sight, it seems that the peak in the curve around 13 K suggests the antiferromagnetic Néel temperature T_N. If this is an indication of the antiferromagnetic Néel temperature, then $ZnFe_2O_4$ has antiferromagnetic long-range order (LRO) below T_N. The magnetic susceptibility curve and the inverse curve have shapes similar to those given in previous reports.[14,15,20] The FC and ZFC curves almost trace the same path over the whole temperature range. Therefore, $ZnFe_2O_4$ is unlike a spin glass system.[1–3,25] Although the data deviate from a Curie-Weiss law for temperatures below 280 K, the Curie-Weiss temperature is 120 K, as estimated from the inverse susceptibility in the high-temperature region. This indicates that ferromagnetic spin correlation dominates at high temperatures. The effective magnetic moment is $4.08\mu_B$, a value that is smaller than expected. However, it does not deviate from trivalency, a fact already confirmed by Mössbauer spectra.[24]

B. Magnetic elastic scattering

Figure 3(a) shows the elastic contour map in the (*HK*0) zone at 15 K. In this figure, solid lines indicate the Brillouin zone boundary (BZB) of the fcc structure. Strong diffuse scattering is distributed along the first BZB, but its location is slightly inside the BZB. The strongest intensity is observed around (0.7, 0.7, 0). Figure 3(b) shows a contour map of the (*HHL*) zone at 15 K. Again, diffuse scattering is distributed along and slightly inside the first BZB. The strongest intensity is also seen around (0.7, 0.7, 0). As described above, the third-neighbor Fe^{3+} ions form an fcc configuration. Therefore, the diffuse scattering pattern indicates that the third-neighbor Fe^{3+} spins are coupled antiferromagnetically, and short-range spin correlations exist between them. Magnetic

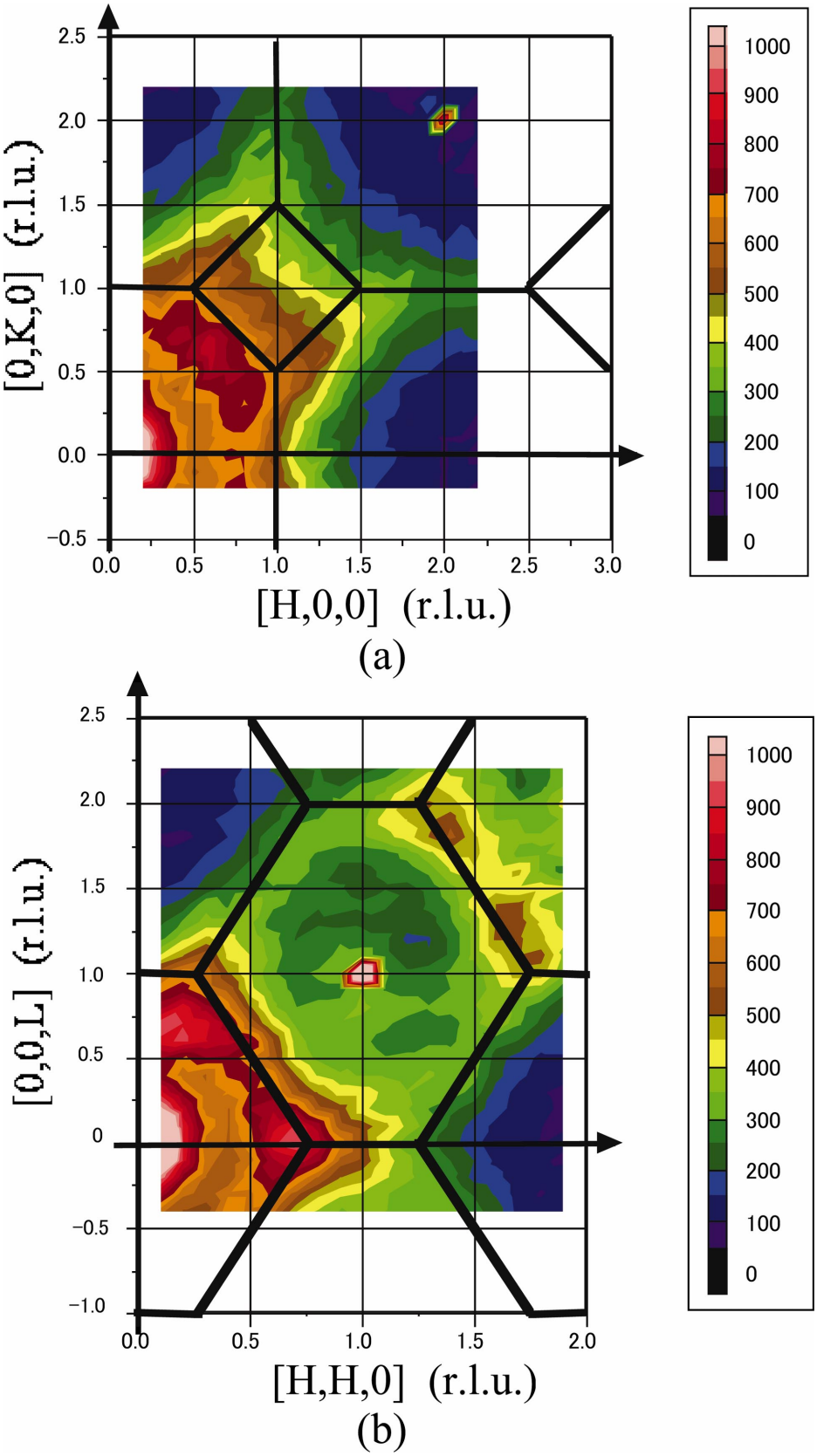

FIG. 3. (Color) Color contour maps of magnetic diffuse scattering in (a) ($HK0$) and (b) (HHL) zones at 15 K. The solid lines indicate the Brillouin zone boundaries of the fcc structure.

scattering along the $[HHH]$ and $[HH0]$ directions at 7, 30, 105, and 299 K, are shown in Figs. 4(a) and 4(b). The lengths of the horizontal axis give the same $|Q|=(H^2+K^2+L^2)^{1/2}$ (Å^{-1}) distance. Another type of diffuse scattering can be seen around the nuclear Bragg peak points. However, at the 220 nuclear Bragg peak there is no diffuse scattering. Table I shows the atomic structure factor for the normal spinel AB_2O_4. For the sake of simplicity, the oxygen contribu-

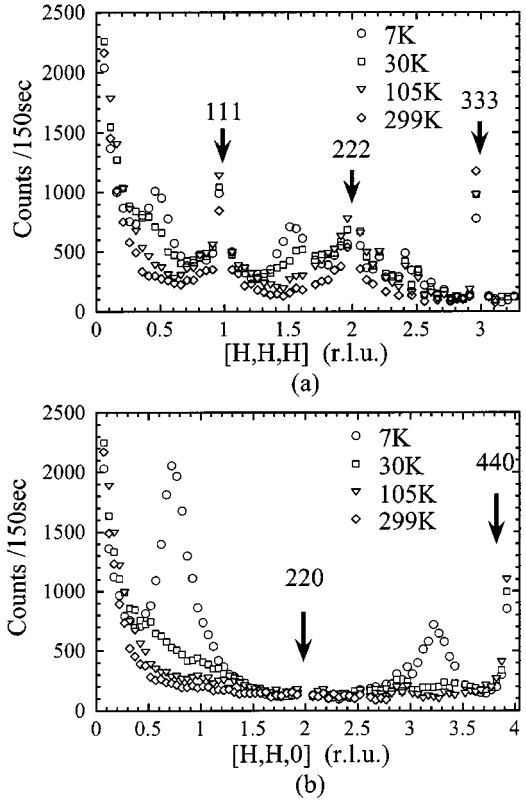

FIG. 4. Magnetic diffuse scattering along (a) the [*HHH*] and (b) [*HH*0] directions for various temperatures.

tion is not described in this table. The diffuse scattering follows the magnetic form factor,[26] and is temperature dependent; therefore, such scattering originates from the magnetic contribution of the *B* atoms. The correspondence between the periodicity of both the magnetic diffuse scattering and the nuclear Bragg peaks, the latter due only to *B* atoms, implies that the former has it roots in the ferromagnetic correlation between Fe^{3+} spins. The diffuse scattering linewidth provides an estimate for the correlation length, namely, 5.11 Å at 30 K, which is within the distance between the second-neighbor Fe^{3+} ions (5.16 Å). Therefore, magnetic diffuse scattering originates from the ferromagnetic coupling of the first-neighbor Fe^{3+} spins. It seems that ferromagnetic diffuse scattering has a maximum intensity at 105 K, while antiferromagnetic diffuse scattering no longer exists there. At low temperatures, the former gradually disappears. Figures 5(a) and 5(b) show the contour maps of the (*HK*0) and (*HHL*) zones at 1.5 K, respectively. Here, the measurement time (counts/60 sec) is the same as that in Fig. 3. Strong diffuse scattering appears at $(1, \frac{1}{2}, 0)$, $(\frac{3}{4}, \frac{3}{4}, 0)$, $(\frac{1}{4}, \frac{1}{4}, 1)$, and symmetrical positions. The temperature variation of the diffuse scattering profiles, that pass through the points $(\frac{1}{2}, 1, 0)$ and $(1, \frac{1}{2}, 0)$, is shown in Fig. 6(a). The linewidth is far broader than that for a nuclear Bragg peak, even at 1.5 K. This indicates that the $(1, \frac{1}{2}, 0)$ peak is a short-range order (SRO) peak. In addition, the $(1, \frac{3}{2}, 0)$ peak, which is seen in powder neutron diffraction measurements, does not appear, even at 1.5 K. Figure 6(b) shows the temperature dependence of the diffuse scattering intensities at $(1, \frac{1}{2}, 0)$, with $k_i = 2.5579\ \text{Å}^{-1}$ and $k_f = 1.0815\ \text{Å}^{-1}$. This figure indicates that the relaxation times are less than 10^{-10} sec.[25] Note, that there is no drastic change in the neutron scattering results around 13 K. Therefore, it is difficult to give the peak in the susceptibility curve at 13 K an Néel temperature interpretation. Diffuse scattering along the ⟨110⟩ axis is shown in Fig. 7(a). As temperature decreases, the scattering center shifts towards the $(\frac{3}{4}, \frac{3}{4}, 0)$ point, with increasing intensity. The same trend is observed for the scan along the ⟨100⟩ axis. Figure 7(b) shows how the maximum peak position and the linewidth vary with temperature. These quantities were determined by a Lorentzian fitting to the data. The linewidth is sensitive to temperature.

TABLE I. Atomic structure factor for the normal spinel AB_2O_4. For simplicity, the oxygen contribution has been omitted. (002 and 442 reflections are forbidden.)

Bragg peak	Atomic structure factor
111, 331	$B-A/\sqrt{2}$
220, 224	A
004, 444	$2B-A$
113, 333	$B+A/\sqrt{2}$
222	$2B$
440	$2B+A$

C. Energy spectra

Figure 8 displays the energy spectra obtained at several reciprocal lattice points for various temperatures. The letters within parentheses in this figure correspond to the letters in the reciprocal space shown in Fig. 9. Even with the very high-energy resolution, the antiferromagnetic diffuse scattering is observed as elastic peaks. On the other hand, inelastic peaks are seen around nuclear Bragg peak positions, e.g., (0.8, 0.8, 0.8) [see Fig. 8(h)]. The data reveals a very soft dispersion relation originating from the antiferromagnetic diffuse scattering position at low temperatures. Figure 10 shows the $|Q'|$ dependences of the inelastic peak center and the linewidth (FWHM), both of which were determined from the data of Fig. 8 by using the ''damped harmonic oscillator (DHO) peak.'' The horizontal $|Q'|$ axis gives the distances from $(1, \frac{1}{2}, 0)$. The letters within parentheses in Fig. 10 also correspond with the letters in the reciprocal space displayed in Fig. 9. The details of the fitting procedure are described in the next section. The inelastic peak centers have maximum values at reciprocal lattice points (2, 2, 0), (2, 0, 0), and (1, 1, 1), where antiferromagnetic diffuse scattering shows its minimum intensity. With increasing temperature, the inelastic peaks gradually shift toward $E=0$ meV. At high temperatures they become quasielastic peaks.

IV. DISCUSSION AND CONCLUSION

In previous work,[12–17] the following issues remained unresolved. (1) the origin of magnetic LRO and SRO, and their coexistence at $(1, \frac{1}{2}, 0)$ and around $(1, \frac{1}{2}, 0)$, respectively, in the low-temperature region. (2) The difference between the

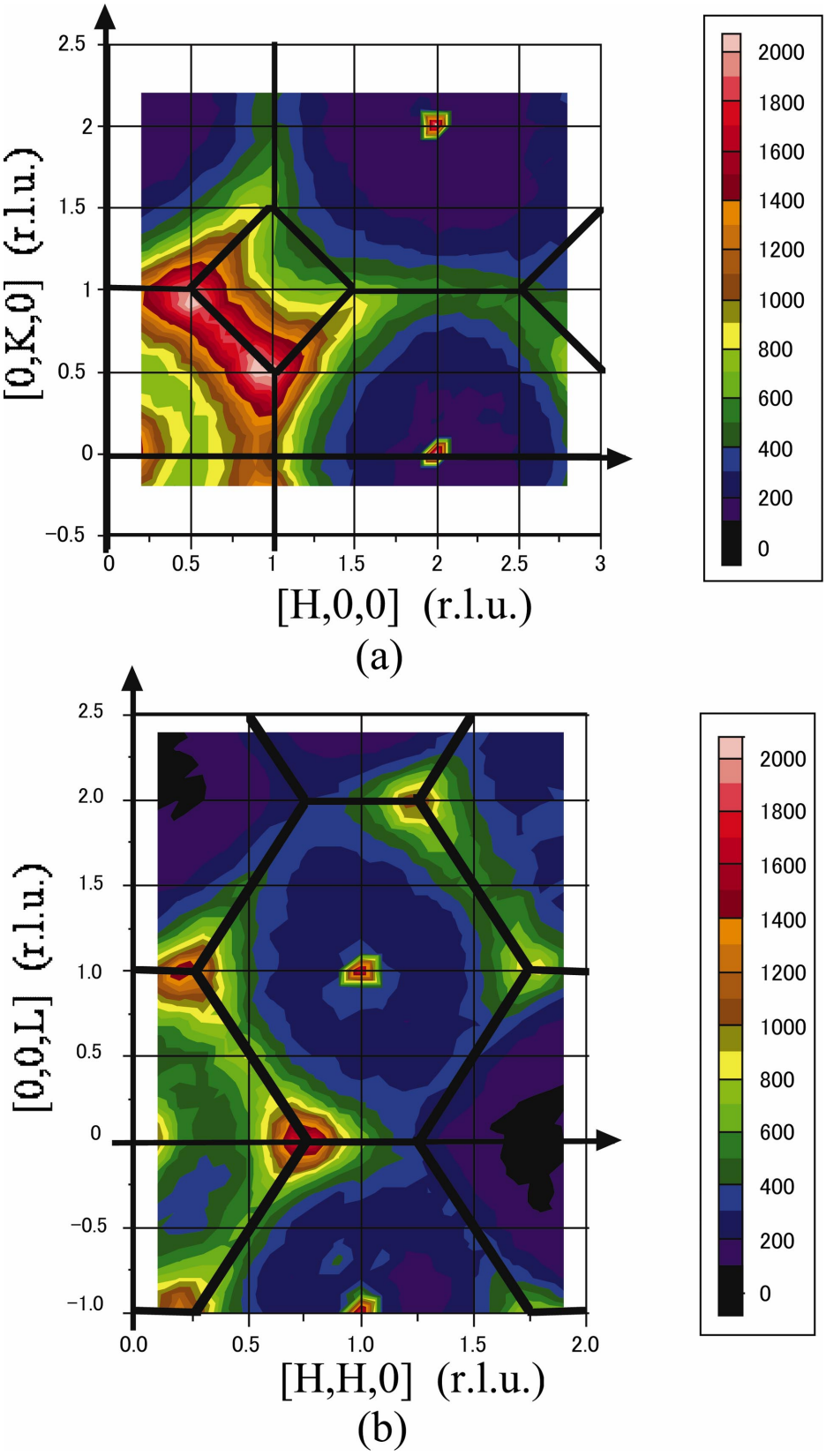

FIG. 5. (Color) Color contour maps of magnetic diffuse scattering in the (a) (*HK*0) and (b) (*HHL*) zones at 1.5 K. The solid lines indicate Brillouin zone boundaries of the fcc structure. Here, the measurement time (counts/60 sec) is the same as that in Fig. 3.

low- and high-temperature patterns of magnetic diffuse scattering, and its position dependence on temperature. Consider the first of these. LRO is related to sample quality. In a previous study,[24] powder neutron diffraction, magnetic susceptibility, and the Mössbauer effect were used to investigate the relationship between sample quality and LRO. In that study, impure samples showed LRO at (1, $\frac{1}{2}$, 0), (1, $\frac{3}{2}$, 0), and equivalent positions, however, magnetic LRO could not be

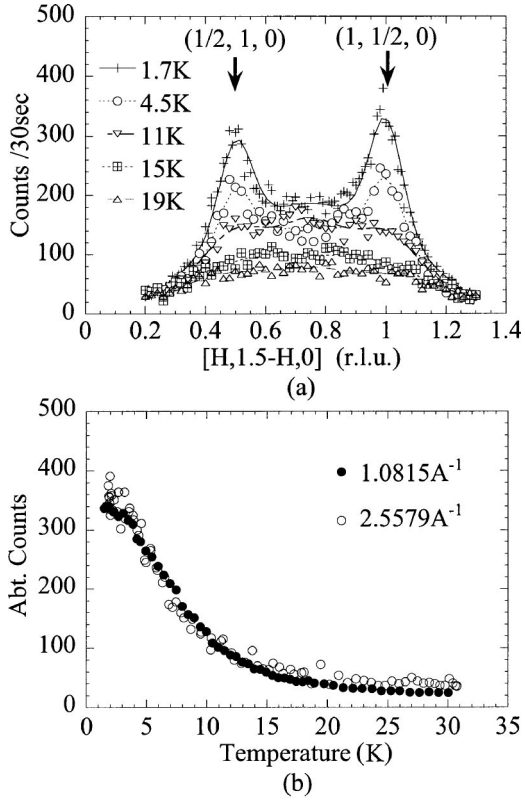

FIG. 6. (a) Magnetic diffuse scattering, passing through (1, $\frac{1}{2}$, 0) and ($\frac{1}{2}$, 1, 0), at various temperatures. (b) The temperature dependence of the peak intensity at (1, $\frac{1}{2}$, 0) with wave vectors $k_i = 2.5579$ Å^{-1} and $k_f = 1.4752$ Å^{-1}.

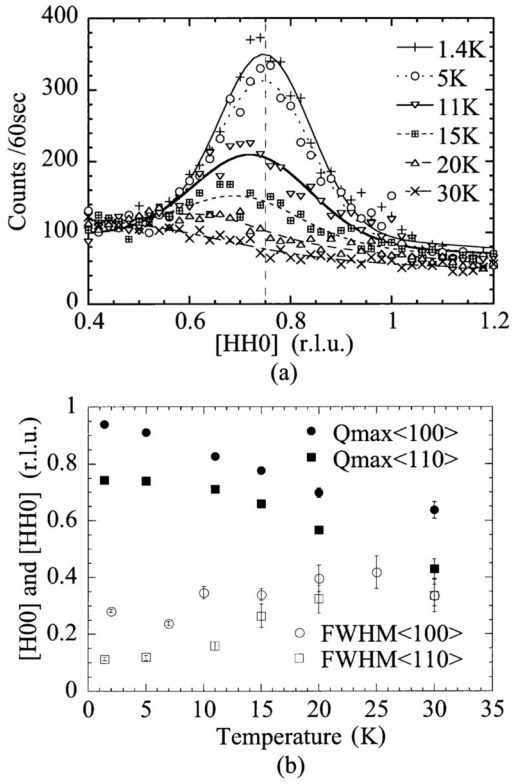

FIG. 7. (a) Enlargement of the Q scan along the $[HH0]$ direction, showing the temperature dependence of antiferromagnetic diffuse scattering. (b) The temperature dependence of the FWHM and the Q positions of the diffuse peak in the $[H00]$ and $[HH0]$ directions.

confirmed with a high-quality powder sample, even at 1.5 K. Only strong magnetic diffuse scattering was obtainable around (1, $\frac{1}{2}$, 0). Consequently, it was revealed that certain sample disorder releases the frustration, and causes long-range spin-correlations. As stated in Sec. I, there is essentially no occurrence of LRO in the present pure-sample system, and there is no Néel temperature. Short-range order arises because spin correlation cannot develop fully in the presence of geometrical frustration. Details of the model that reproduces the magnetic diffuse scattering patterns for $^{110}CdFe_2O_4$ and $ZnFe_2O_4$ will be published elsewhere.[27]

In this regard, the application of spin clusters is a reasonable approach (e.g., hexagon model; Ref. 8). We turn now to the second issue listed above. The origin of temperature-dependent magnetic diffuse scattering patterns is explained by the competition between the third-neighbor interactions and temperature dependence of the first-neighbor interactions. Although it is usually difficult to think of a temperature-dependent interaction, the interaction in the present system effectively depends on the temperature. (See Ref. 28 for details.) Also, although it is unusual that the third-nearest neighbor interaction is stronger than that of the first-nearest neighbor, these interactions are based on the following unique property. Up to now, the nearest-neighbor Fe^{3+}-O-Fe^{3+} exchange interactions in the 90° configuration have been considered to be antiferromagnetic or unclarified.[29–32] (Here, both superexchange and the direct-exchange interactions are taken into account.) With the present results, we were able to obtain precise information concerning the sign of the interaction. The first-neighbor exchange interaction is ferromagnetic when the Fe^{3+}-O-Fe^{3+} angle is 95°. Since the strength of the interaction is very weak, we consider it to be almost paramagnetic.[32] As temperature decrease, the Fe^{3+}-O-Fe^{3+} angle is increasing gradually, and the strength of the ferromagnetic first-neighbor interaction decreases. On this basis, we can expect that the sign of the interaction varies from ferromagnetic to antiferromagnetic as the Fe^{3+}-O-Fe^{3+} angle increases. In fact, we confirmed that the first-neighbor exchange interaction is antiferromagnetic when the Fe^{3+}-O-Fe^{3+} angle is 98°. The details of our recent neutron-scattering results for the isotope $^{110}CdFe_2O_4$ will be published elsewhere.[27] Its diffuse scattering pattern is the same as those for $ZnCr_2O_4$ (Ref. 9) and $Y(Sc)Mn_2$,[7] indicating that the first-neighbor exchange Fe^{3+}-O-Fe^{3+} interaction is antiferromagnetic, and that the frustration occurs within the tetrahedron. Under such a unique condition, the first-neighbor direct-exchange and superexchange interactions almost nullify each other, which means that the third-neighbor interaction becomes the dominant one, and unusual magnetic behavior ensues. With the choice of other samples, that have proper angles between magnetic atoms, we can expect behavior similar to that found in the present case.

At first sight, the diffuse scattering pattern of $ZnFe_2O_4$ is

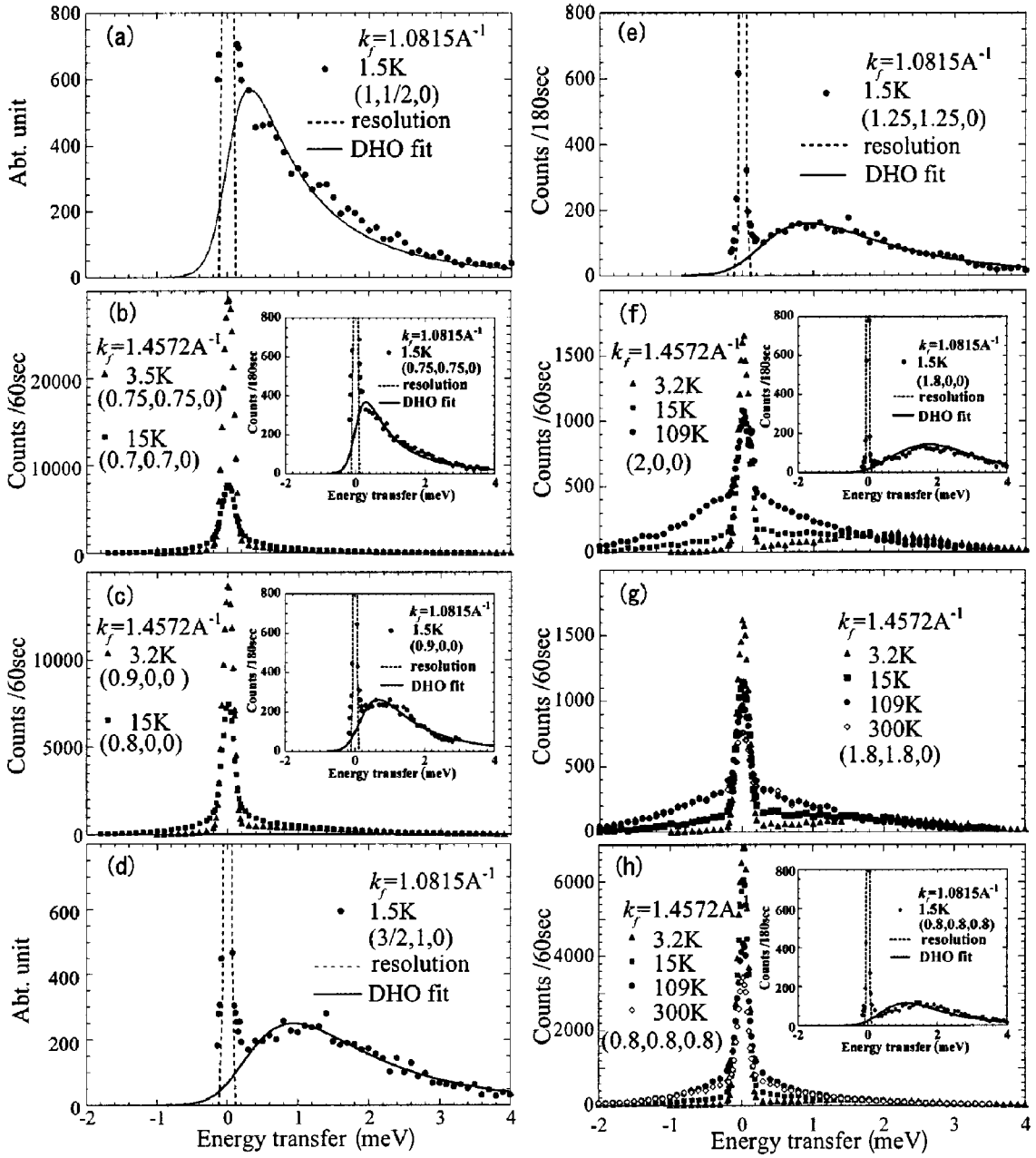

FIG. 8. Energy spectra obtained at several temperatures and reciprocal lattice points using two wavelengths: (a) $T=1.5$ K at $(1, \frac{1}{2}, 0)$ with $k_f=1.0815$ Å^{-1}, (b) $T=3.5$ K at $(\frac{3}{4}, \frac{3}{4}, 0)$, and $T=15$ K at (0.7, 0.7, 0) with $k_f=1.4572$ Å^{-1} [(b) inset] $T=1.5$ K at $(\frac{3}{4}, \frac{3}{4}, 0)$ with $k_f=1.0815$ Å^{-1}, (c) $T=3.2$ K at (0.9, 0, 0) and $T=15$ K at (0.8, 0, 0) with $k_f=1.4572$ Å^{-1} [(c) inset] $T=1.5$ K at (0.9, 0, 0) with $k_f=1.0815$ Å^{-1}, (d) $T=1.5$ K at $(\frac{3}{2}, 1, 0)$ with $k_f=1.0815$ Å^{-1}, (e) $T=1.5$ K at $(\frac{5}{4}, \frac{5}{4}, 0)$ with $k_f=1.0815$ Å^{-1}, (f) $T=3.2$, 15, and 109 K at (2, 0, 0) with $k_f=1.4572$ Å^{-1} [(f) inset] $T=1.5$ K at (1.8, 0, 0) with $k_f=1.0815$ Å^{-1}, (g) $T=3.2$, 15, 109, and 300 K at (1.8, 1.8, 0) with $k_f=1.4572$ Å^{-1}, (h) $T=3.2$, 15, 109, and 300 K at (0.8, 0.8, 0.8) with $k_f=1.4572$ Å^{-1} and [(h) inset] $T=1.5$ K at (0.8, 0.8, 0.8) with $k_f=1.0815$ Å^{-1}. The solid line in each figure corresponds to values calculated from Eq. (2). The dashed line in each figure represents the resolution observed with vanadium as standard. The letters within parentheses correspond to letters in the reciprocal space of Fig. 9.

very similar to that of spin ice systems, e.g., $Ho_2Ti_2O_7$ (Refs. 4 and 5). However, there is a difference between the present system and spin ice systems,[4–6] as seen in their respective magnetic diffuse scattering patterns. Unlike the spin ice system $Ho_2Ti_2O_7$ which exhibits four-leaf diffuse scattering, there are strong diffuse peaks in $ZnFe_2O_4$, which appear not only at $(\frac{3}{4}, \frac{3}{4}, 0)$, but also at $(\frac{1}{4}, \frac{1}{4}, 1)$ and symmetrical points. The origin of spin ice is explained by the dipole interaction,[33–39] which leads to ferromagnetic coupling between the first-neighbor spins. However, the $ZnFe_2O_4$ pattern can be reproduced successfully without the dipole interaction (see Ref. 28). In addition, the dipole interaction cannot explain the results for $CdFe_2O_4$. In view of our $^{110}CdFe_2O_4$ experiments (Ref. 27), it is difficult to apply the dipole interaction to the present data. The issues concerning magnetic susceptibility data are also explained reasonably

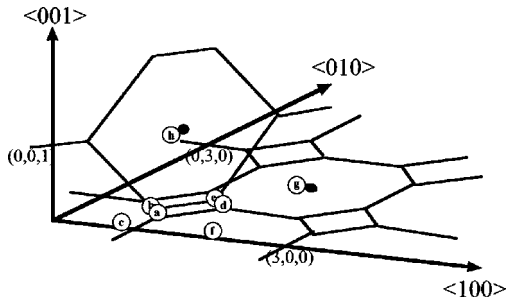

FIG. 9. Diagram of reciprocal space for $ZnFe_2O_4$. The open circles (labeled with letters) indicate positions where we observed energy spectra. The solid circles indicate nuclear reflections, and the solid lines denote Brillouin zone boundaries of the fcc structure.

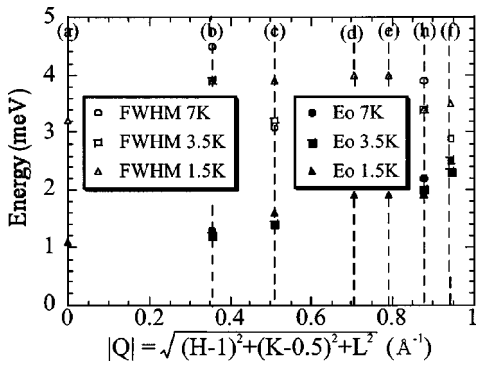

FIG. 10. The $|Q'|$ dependences of the inelastic peak center and the linewidth (FWHM), which were determined from the data in Fig. 8 using the ''damped harmonic oscillator (DHO) peak.'' The horizontal $|Q'|$ axis gives the distances from (1, $\frac{1}{2}$, 0). The letters within parentheses in Fig. 10 correspond to letters in the reciprocal space of Fig. 9.

well by the competition between the third-neighbor interactions and temperature dependence of the first-neighbor interactions. We consider that the deviation from a Curie-Weiss law below 100 K arises from the antiferromagnetic component, which gradually dominates at low temperature, while the ferromagnetic component dominates at high temperature. As for the peak around 13 K, it is difficult to attribute it to any magnetic transition, since neutron scattering measurements do not show any drastic change there. In almost all normal spinels, there is a similar peak below 50 K. However, we cannot resolve this issue for $ZnFe_2O_4$. It may be a peak caused by a slight lattice distortion,[40,41] although none could be detected.

The effective numbers of Bohr magnetons per magnetic ion (obtained from high-temperature susceptibilities), and commonly seen for other frustrated systems, are smaller than the expected values. We reason that the magnetic moment is not actually shorten, because Mössbauer spectra already show that the Fe atom is trivalent.[21]

The energy spectrum analysis also reveals that there is no LRO in $ZnFe_2O_4$. After the correction for instrument resolution, the energy spectrum is analyzed as the sum of two components: an ''elastic'' Gaussian peak, including elastic incoherent scattering, and an ''inelastic'' damped harmonic oscillator (DHO) peak, given by the functional forms

$$I(Q,\omega) \propto \frac{\omega}{1-\exp(-\hbar\omega/kT)} \exp\left\{-\frac{\omega^2}{2\Gamma_1^2}\right\}, \qquad (1)$$

$$I(Q,\omega) \propto \frac{\omega}{1-\exp(-\hbar\omega/kT)} \frac{\omega_0^2\Gamma_2}{(\omega^2-\omega_0^2)^2+\omega^2\Gamma_2^2}, \qquad (2)$$

respectively, where ω_0 is the peak center, Γ_1 and Γ_2 are FWHM, and T is temperature.

There is a very soft dispersion relation, which is difficult to observe with the constant-E scan mode.[42] At low temperature, the dispersion relations extend from the antiferromagnetic diffuse scattering position, and the corresponding zone boundary is defined by the nuclear Bragg peak positions. Alternatively, at high temperature, the dispersion relations extend from the nuclear Bragg peak positions to the zone boundary which is defined by the antiferromagnetic diffuse scattering position. However, this could not be confirmed because of thermal fluctuations. Also, it is thought that the energy spectra vary from antiferromagnetic to ferromagnetic.

Energy spectra consist of elastic and inelastic scattering components (see Fig. 8). The spin dynamics, characterized by magnetic diffuse scattering, is observed as an elastic peak in the energy spectra, even when a cold neutron source is used. However, the elastic peak does not literally imply a static state. Upon considering the time scale of neutron scattering and that of the Mössbauer effect,[21] it turns out that the relaxation time is of the order of $10^{-7}-10^{-10}$ sec.

The characteristic time deduced from the inelastic peak is 10^{-12} sec. This mode is almost obscure and mixed with the relaxation time. The inelastic peaks are too broad to be identified as magnons. These peaks are thought to be reminiscent of magnons, because LRO is suppressed by the frustration effect. This also indicates that there is essentially no LRO in the present system. These characteristics of the spectrum are close to those of the ''jumped diffusion model'' which is usually used for a liquid. This indicates that $ZnFe_2O_4$ is a spin liquid,[43] rather than a spin glass.

We conclude that SRO and spin fluctuations result from the geometrical-frustration effect. The origin of the unusual magnetic behavior of $ZnFe_2O_4$ arises from this frustration and a unique property of the first-neighbor interaction.

[1] M. J. P. Gingras, C. V. Stager, N. P. Raju, B. D. Gaulin, and J. E. Greedan, Phys. Rev. Lett. **78**, 947 (1997).

[2] J. S. Gardner, B. D. Gaulin, S.-H. Lee, C. Broholm, N. P. Raju, and J. E. Greedan, Phys. Rev. Lett. **83**, 211 (1999).

[3] Amit Keren and Jason S. Gardner, Phys. Rev. Lett. **87**, 177201 (2001).

[4] S. T. Bramwell, M. J. Harris, B. C. den Hertog, M. J. P. Gingras, J. S. Gardner, D. F. McMorrow, A. R. Wildes, A. L. Cornelius, J.

D. M. Champion, R. G. Melko, and T. Fennel, Phys. Rev. Lett. **87**, 047205 (2001).
[5] Masaki Kanada, Yukio Yasui, Yasuyuki Kondo, Satoshi Iikubo, Masafumi Ito, Hiroshi Harashina, Matatoshi Sato, Hajime Okumura, Kazuhusa Kakurai, and Hiroaki Kadowaki, J. Phys. Soc. Jpn. **71**, 313 (2002).
[6] H. Kadowaki, Yoshinobu Ishii, Kazuyuki Matsuhira, and Yukio Hinatsu, Phys. Rev. B **65**, 144421 (2002).
[7] R. Ballou and E. Lelièvre-Berna, Phys. Rev. Lett. **76**, 2125 (1996).
[8] K. Kamazawa, Y. Tsunoda, K. Odaka, and K. Kohn, J. Phys. Chem. Solids **60**, 1261 (1999).
[9] S.-H. Lee, C. Broholm, W. Ratcliff, G. Gaasparovic, G. Huang, T. H. Kim, and S.-W. Cheong, Nature (London) **418**, 856 (2002).
[10] J. S. Gardner, B. D. Gaulin, A. J. Berlinsky, P. Waldron, S. R. Dunsiger, N. P. Raju, and J. E. Greedan, Phys. Rev. B **64**, 224416 (2001).
[11] S.-H. Lee, C. Broholm, Y. Ueda, and J. J. Rush, Phys. Rev. Lett. **86**, 5554 (2001).
[12] D. M. Grimes and Edger F. Westrum, Jr., J. Appl. Phys. **29**, 384 (1958).
[13] J. M. Hastings and L. M. Corliss, Phys. Rev. **15**, 1460 (1956).
[14] S. Ligenza, Phys. Status Solidi B **75**, 315 (1976).
[15] Yu. G. Chukalkin and V. R. Shtirts, Fiz. Tverd. Tela (Leningrad) **30**, 2919 (1988) [Sov. Phys. Solid State **30**, 1683 (1988)].
[16] W. Schiessl, W. Potzel, H. Karzel, M. Steiner, and G. M. Kalvius, Phys. Rev. B **53**, 9143 (1996).
[17] B. Boucher, R. Buhl, and M. Perrin, Phys. Status Solidi **40**, 171 (1970).
[18] P. W. Anderson, Phys. Rev. **102**, 1008 (1956).
[19] S. T. Bramwell and M. J. Harris, J. Phys.: Condens. Matter **10**, L215 (1998).
[20] F. K. Lotgering, J. Phys. Chem. Solids **27**, 139 (1966).
[21] U. Köning, E. F. Bertaut, Y. Gros, and G. Chol, Solid State Commun. **8**, 759 (1970).
[22] V. G. Vologin, Fiz. Tverd. Tela (Leningrad) **29**, 2323 (1987) [Sov. Phys. Solid State **29**, 1339 (1987)].
[23] Yu. G. Chukalkin, V. R. Shtirts, and B. N. Goshchitskil, Fiz. Tverd. Tela (Leningrad) **30**, 3201 (1988) [Sov. Phys. Solid State **30**, 1841 (1988)].
[24] T. Usa, K. Kamazawa, S. Nakamura, H. Sekiya, Y. Tsunoda, K. Kohn, and M. Tanaka, in Proceedings of the Eighth International Conference on Ferrite, Kyoto, Japan, 2000, edited by M. Abe and Y. Yamazaki, p. 316.
[25] S. A. Werner, J. J. Rhyne, and J. A. Gotaas, Solid State Commun. **56**, 457 (1985).
[26] R. E. Watson and A. J. Feeman, Acta Crystallogr. **14**, 27 (1961).
[27] K. Kamazawa, S. Park, T. J. Sato, S.-H. Lee, and Y. Tsunoda (unpublished).
[28] Y. Yamada, K. Kamazawa, and Y. Tsunoda, Phys. Rev. B **66**, 064401 (2002).
[29] Junjiro Kanamori, J. Phys. Chem. Solids **10**, 87 (1959).
[30] P. W. Anderson, Phys. Rev. **115**, 2 (1959).
[31] Ken-Ichiro Gondaira and Yukito Tanabe, J. Phys. Soc. Jpn. **21**, 1527 (1966).
[32] Kiyosi Motida and Syôhei Miyahara, J. Phys. Soc. Jpn. **28**, 1188 (1970).
[33] M. J. Harris, S. T. Bramwell, D. F. McMorrow, T. Zeiske, and K. W. Godfrey, Phys. Rev. Lett. **79**, 2554 (1997).
[34] R. Siddharthan, B. S. Shastry, A. P. Ramirez, A. Hayashi, R. J. Cava, and S. Rosenkranz, Phys. Rev. Lett. **83**, 1854 (1999).
[35] M. J. Harris, S. T. Bramwell, P. C. W. Holdsworth, and J. D. M. Champion, Phys. Rev. Lett. **81**, 4496 (1998).
[36] Byron C. den Hertog and Michel. J. P. Gingras, Phys. Rev. Lett. **84**, 3430 (2000).
[37] R. G. Melko, Byron C. den Hertog, and Michel. J. P. Gingras, Phys. Rev. Lett. **87**, 067203 (2001).
[38] G. Blasse, Philips Res. Rep. **18**, 383 (1963).
[39] S. B. Berger, J. I. Budnick, and T. J. Burch, Phys. Rev. **10**, 179 (1969).
[40] S.-H. Lee, C. Broholm, T. H. Kim, W. Ratcliff II, and S.-W. Cheong, Phys. Rev. Lett. **84**, 3718 (2000).
[41] Oleg Tchernyshyov, R. Moessner, and S. L. Sondhi, Phys. Rev. Lett. **88**, 067203 (2002).
[42] K. Kamazawa, Y. Tsunoda, K. Odaka, and K. Kohn, in Proceedings of the Eighth International Conference on Ferrite (Ref. 24), p. 217.
[43] P. A. Egelstaff, *An Introduction to the Liquid State* (Academic Press, London, 1967).